Supplementary Information for

Tracking and quantification of dendritic cell migration and antigen trafficking between the skin and lymph nodes

Michio Tomura, Akihiro Hata, Satoshi Matsuoka, Francis H.W. Shand, Yasutaka Nakanishi, Ryoyo Ikebuchi, Satoshi Ueha, Hidekazu Tsutsui, Kayo Inaba, Kouji Matsushima, Atsushi Miyawaki, Kenji Kabashima, Takeshi Watanabe, and Osami Kanagawa

Supplementary Figure S1. The gene targeting strategy used to generate ROSA26-CAG-loxP-stop-loxP-KikGR knock-in mice.

Supplementary Figure S2. Identification of skin-derived DC subsets in the lymph node (LN), epidermis and dermis by flow cytometry.

Supplementary Figure S3. Identification of skin-derived DC subsets in the dLN using Langerin-EGFP mice and flow cytometry.

Supplementary Figure S4. Identification of LCs in the LNs of KikGR chimeric mice by flow cytometry.

Supplementary Figure S5. Migration of KikGR-red skin-derived DCs to the auricular dLNs after photoconversion of the skin of the ears.

Supplementary Figure S6. Repeat photoconversion of the abdominal skin to determine the proportion of the photoconverted skin area that is drained by the dLN.

Supplementary Figure S7. Summary of the dynamics of skin-derived DC migration and antigen trafficking in the steady state, after chemical stress, and after mechanical injury.

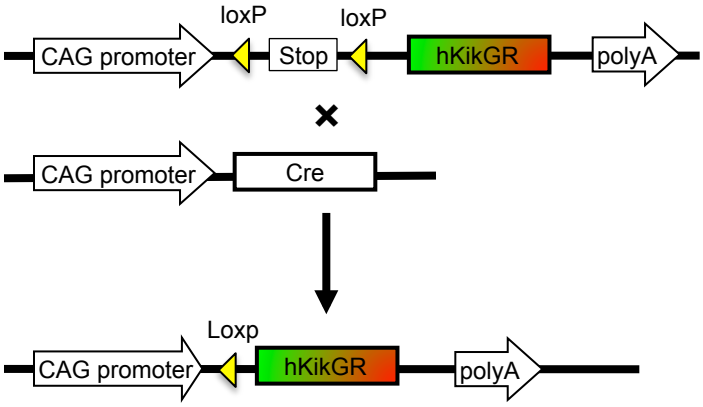

Supplementary Figure S1. The gene targeting strategy used to generate ROSA26-CAG-loxP-stop-loxP-KikGR knock-in mice. ROSA26-CAG-loxP-stop-loxP-KikGR knock-in mice were cross-mated with CAG-Cre mice to delete the loxP-stop-loxP site and achieve KikGR expression in all cells of the mice due to the ubiquitous expression of the CAG promoter.

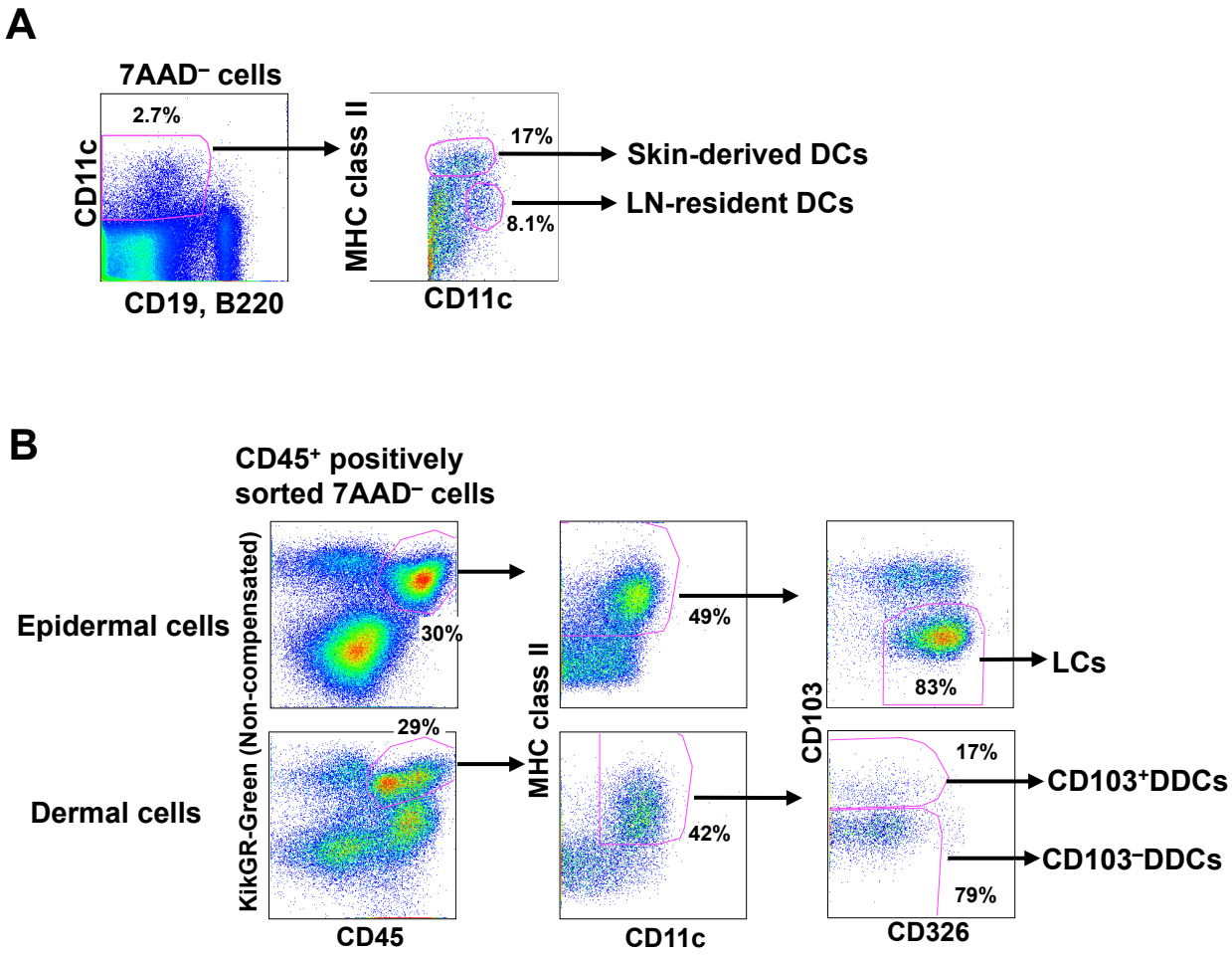

Supplementary Figure S2. Identification of skin-derived DC subsets in the lymph node (LN), epidermis and dermis by flow cytometry. (**A**) Gating scheme used to identify skin-derived DCs and LN-resident DCs in the dLN. Single-cell suspensions from the LNs of KikGR mice were incubated with an Fc-blocker (2.4G2), stained with a biotinylated anti-CD103 antibody followed by PE/Cy7-conjugated anti-CD19 and anti-B220 antibodies, APC-conjugated streptavidin, an APC/Cy7-conjugated anti-CD326 antibody, a Pacific Blue-conjugated anti-CD11c antibody, and a Pacific Orange-conjugated anti-MHC class II antibody, after which the cells were analyzed by flow cytometry. Dead cells were excluded based on 7-amino-actinomycin D (7AAD) staining. (**B**) Gating scheme used to identify LCs in the epidermis and CD103⁻DDCs and CD103⁺ DDCs in the dermis. Single-cell suspensions from the epidermis and dermis of KikGR mice were incubated with an Fc-blocker (2.4G2), then stained with anti-CD45 MACS beads for positive selection-based enrichment of CD45⁺ cells using a MACS column. CD45⁺ cells were then stained with a biotinylated anti-CD103 antibody followed by PE/Cy7-conjugated anti-CD45, APC-conjugated anti-MHC class II, APC/Cy7-conjugated anti-CD326, Brilliant Violet 421-conjugated anti-CD103, and Brilliant Violet 570-conjugated CD11c antibodies. Dead cells were excluded based on 7-amino-actinomycin D (7AAD) staining.

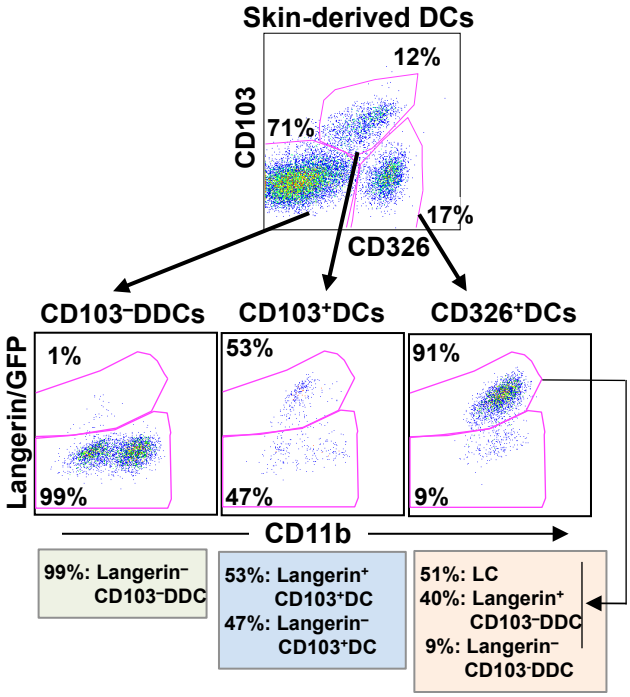

Supplementary Figure S3. Identification of skin-derived DC subsets in the dLN using Langerin-EGFP mice and flow cytometry. Single-cell suspensions from the cutaneous LNs of Langerin-EGFP mice were stained with fluorochrome-labeled anti-CD103, anti-CD11b, anti-CD326, anti-CD11c, anti-MHC class II, anti-CD19, and anti-B220 antibodies before analysis by flow cytometry. Dead cells were excluded based on 7-amino-actinomycin D (7AAD) staining. After gating as shown in **Supplementary Fig. S2A**, skin-derived DCs were gated into subpopulations based on their expression of CD103 and CD326. Lower plots show the expression of Langerin/GFP and CD11b within each subpopulation. Percentages on dot plots indicate the frequency of each subset. Data are representative of three independent experiments.

*$CD103^-$DDCs consisted almost entirely of $Langerin^-CD103^-$DDCs.

*$CD103^+$DCs consisted of 47% $Langerin^-CD103^+$DCs and 53% $Langerin^+$ $CD103^+$ DCs.

*$CD326^+$DCs consisted of 9% $Langerin^-CD103^-$DDCs and 91% $Langerin^+$ cells. The $Langerin^+$ cells could be further divided into 51% LCs and 40% (91% minus 51%) $CD103^-Langerin^+$DDCs, because $CD326^+$DCs represented 51% of LCs (see **Supplementary Fig. S4**) and LCs express Langerin.

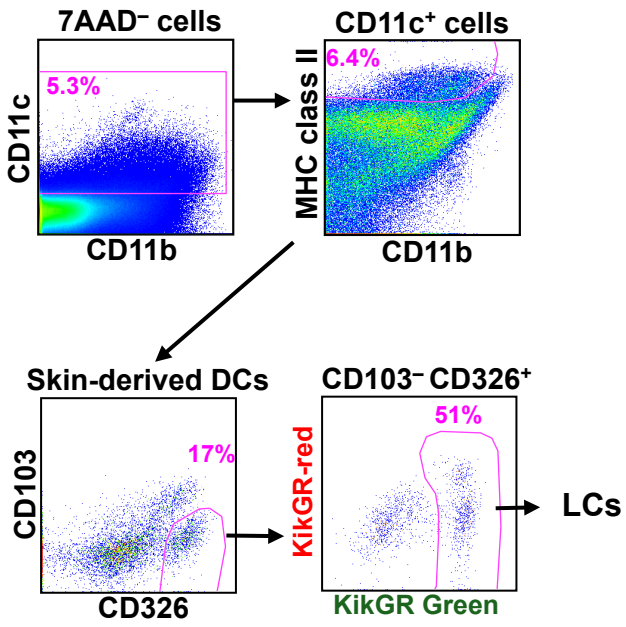

Supplementary Figure S4. Identification of LCs in the LNs of KikGR chimeric mice by flow cytometry. BM chimeras in which KikGR mice were reconstituted with BM cells from WT mice (WT BM→KikGR) were used to detect radioresistant LCs. Single-cell suspensions of LNs from WT-BM→KikGR chimeric mice were incubated with a Fc-blocker (2.4G2), stained with PE/Cy7-conjugated anti-CD11b, APC-conjugated anti-MHC class II, APC/Cy7-conjugated anti-CD326, Brilliant Violet 421-conjugated anti-CD103 and Brilliant Violet 570-conjugated CD11c antibodies, then analysed by flow cytometry. Dead cells were excluded based on 7-amino-actinomycin D (7AAD) staining. Within the $CD103^{-}CD326^{+}$ subpopulation of $CD11c^{+}$MHC class II^{high} DCs, radioresistant LCs were identified as $KikGR^{+}$ cells.

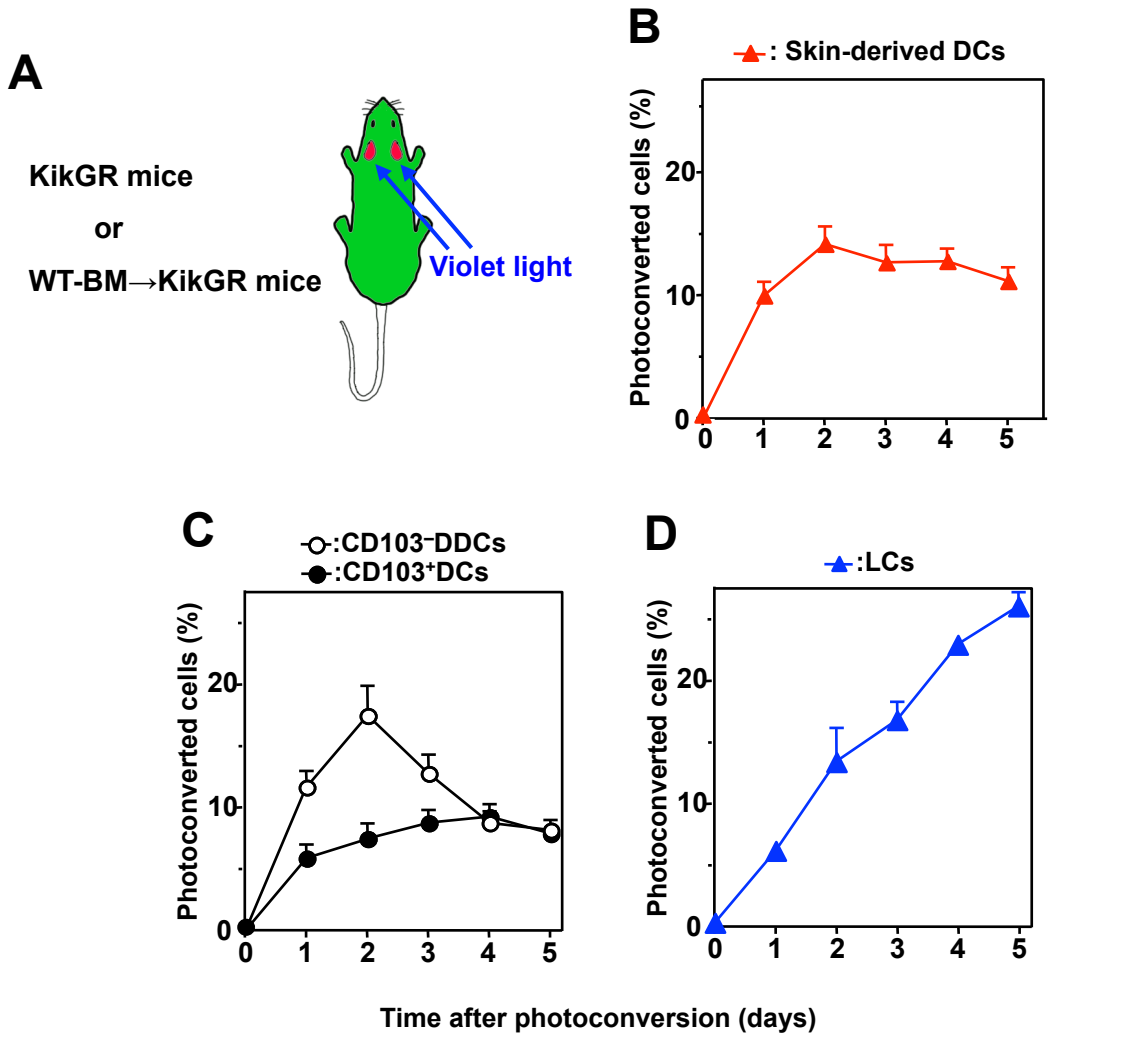

Supplementary Figure S5. Migration of KikGR-red skin-derived DCs in the auricular dLNs after photoconversion of the skin of the ears. (**A**) The ear skin of KikGR mice or WT-BM→KikGR chimeric mice was photoconverted by exposure to violet light (436 nm, 95 mW/cm^2) for 2 min. (**B**) Following ear skin photoconversion, cells from the auricular dLNs were isolated and stained for analysis of skin-derived DCs by flow cytometry (see **Supplementary Fig. S2A** for gating strategy). (**C**) Total skin-derived DCs from the auricular dLN of KikGR mice after ear skin photoconversion (as in panel **B**) were further gated into CD103$^-$DDCs and CD103$^+$DCs (see **Supplementary Fig. S3** for gating strategy). (**D**) The ear skin of WT-BM→KikGR chimeric mice was photoconverted before analysis of LCs in the auricular dLN by flow cytometry (see **Supplementary Fig. S4** for gating strategy). Data (mean ± SE) represent the proportion of skin-derived DCs labeled KikGR-red. A minimum of six samples was analyzed at each time point. Data are representative of two independent experiments. Illustration created by M.T. using Adobe Photoshop software.

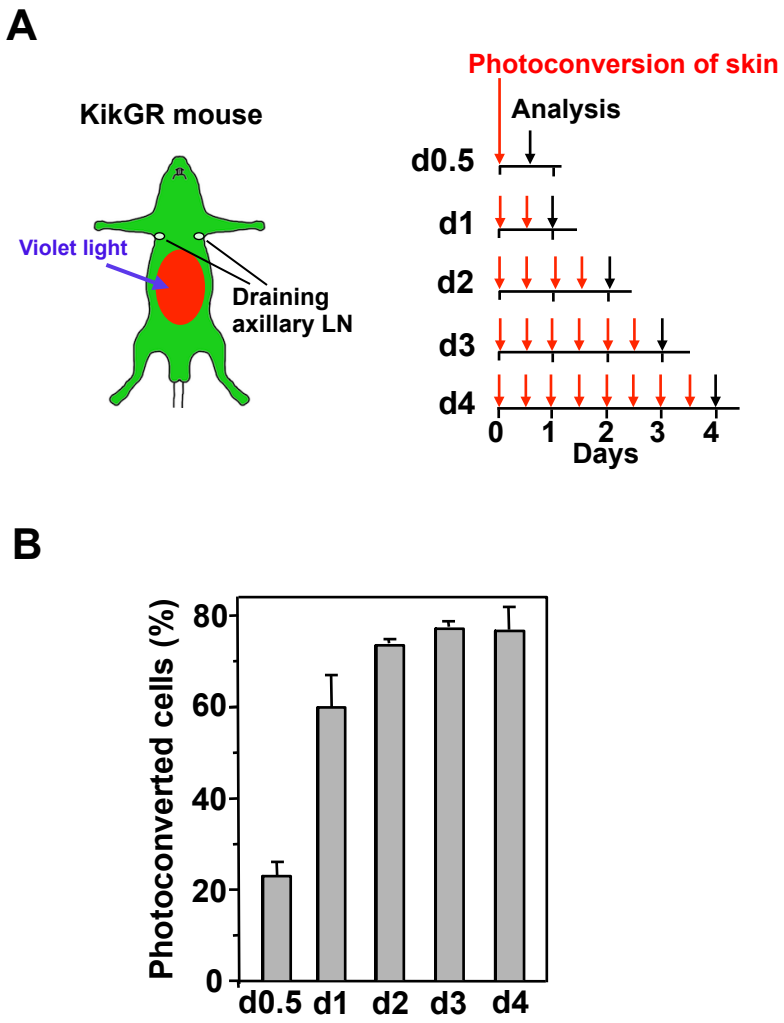

Supplementary Figure S6. Repeat photoconversion of the abdominal skin to determine the proportion of the photoconverted skin area that is drained by the dLN. (**A**) The clipped abdominal skin of KikGR mice was photoconverted every 12 h for 1, 2, 3, or 4 days in order to produce a continuous supply of KikGR-red DCs migrating to the dLN. (**B**) Cells from the dLNs were isolated at the time points indicated and stained for analysis of skin-derived DCs by flow cytometry (see **Supplementary Fig. S2A** for gating strategy). Data represent the proportion of skin-derived DCs labeled KikGR-red. The proportion of KikGR-red skin-derived DCs in the dLN plateaued at 76% ± 5.2% (mean ± SE, n = 3). These results suggest that under our protocol, the abdominal skin "photoconverted area" represented 76% of the skin draining to the axillary dLNs, which is the maximum possible proportion of KikGR-red skin-derived DCs in the dLN. The other 24% of skin-derived DCs in the dLN (KikGR-green) are derived from skin outside the abdominal photoconversion area. Illustration created by M.T. using Adobe Photoshop software.

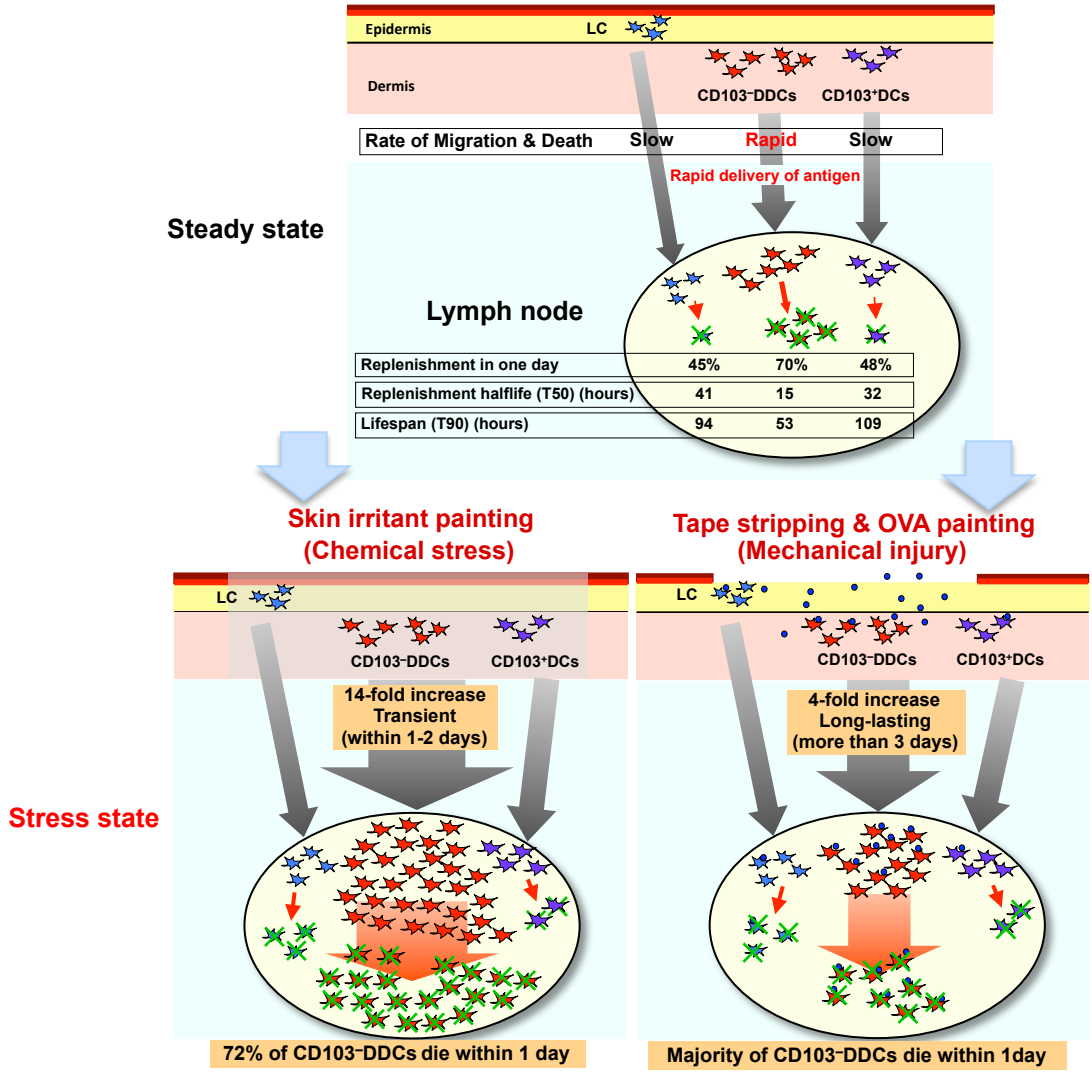

Supplementary Figure S7. Summary of the dynamics of skin-derived DC migration and antigen trafficking in the steady state, after chemical stress, and after mechanical injury. In the steady state, the relative migration rates of skin-derived DC subsets were: CD103⁻DDCs (Langerin⁻CD103⁻DDCs) > CD103⁺DCs (including Langerin⁺CD103⁺DDCs) ≒ LCs. Migration rates correlated with daily replenishment rates and calculated lifespans (upper panel). Skin irritant painting induced a 14-fold increase in CD103⁻DDC migration from the skin to the dLN on day one, however, 72% of these cells were lost from the dLN within the next 24 h (bottom left). Tape stripping promoted the trafficking of exogenous proteins by CD103⁻DDCs and a 4-fold increase in the migration of these cells to the dLNs that lasted for more than three days; however, the majority of migrants were lost and replaced by new migrants within 24 h (bottom right).